INVITED ARTICLE

TECHNOLOGY

Dynamic deformability of sickle red blood cells in microphysiological flow

Y. Alapan[1,*], Y. Matsuyama[1,*], J. A. Little[2,3] & U. A. Gurkan[1,4,5,6]

In sickle cell disease (SCD), hemoglobin molecules polymerize intracellularly and lead to a cascade of events resulting in decreased deformability and increased adhesion of red blood cells (RBCs). Decreased deformability and increased adhesion of sickle RBCs lead to blood vessel occlusion (vaso-occlusion) in SCD patients. Here, we present a microfluidic approach integrated with a cell dimensioning algorithm to analyze dynamic deformability of adhered RBC at the single-cell level in controlled microphysiological flow. We measured and compared dynamic deformability and adhesion of healthy hemoglobin A (HbA) and homozygous sickle hemoglobin (HbS) containing RBCs in blood samples obtained from 24 subjects. We introduce a new parameter to assess deformability of RBCs: the dynamic deformability index (DDI), which is defined as the time-dependent change of the cell's aspect ratio in response to fluid flow shear stress. Our results show that DDI of HbS-containing RBCs were significantly lower compared to that of HbA-containing RBCs. Moreover, we observed subpopulations of HbS containing RBCs in terms of their dynamic deformability characteristics: deformable and non-deformable RBCs. Then, we tested blood samples from SCD patients and analyzed RBC adhesion and deformability at physiological and above physiological flow shear stresses. We observed significantly greater number of adhered non-deformable sickle RBCs than deformable sickle RBCs at flow shear stresses well above the physiological range, suggesting an interplay between dynamic deformability and increased adhesion of RBCs in vaso-occlusive events.

***Keywords*: Microfluidics; Red Blood Cell; Dynamic Cell Deformation; Cell Adhesion; Cell Mechanics; Biomechanics; Sickle Cell Disease.**

INNOVATION

Accurate measurement of RBC deformability and adhesion, which are the two key biophysical factors of vaso-occlusion in sickle cell disease (SCD), holds great potential as a marker for evaluation of disease progression, for gaining insight into disease pathophysiology and for development of novel therapeutics. We developed a versatile microfluidic platform integrated with a cell-dimensioning algorithm for quantitative assessment of dynamic deformability and adhesion of red blood cells (RBCs) in controlled microphysiological flow. The developed microfluidic system can probe deformation characteristics of RBCs at the single-cell level, as well as reflect microvasculature adhesion potential. To assess dynamic deformability of RBCs, we introduced a new parameter: dynamic deformability index (DDI), which is defined as the time dependent change of an adherent cell's aspect ratio in response to fluid shear. Using this microfluidic system, we analyzed dynamic deformability and adhesion of sickle RBCs at physiological and above physiological flow shear stresses. The microfluidic system described here has the potential to be used in a high-throughput manner with an integrated automated image processing algorithm for measurement of RBC deformability and adhesion in patients' blood.

INTRODUCTION

RBCs undergo dynamic reversible deformations in blood circulation and respond to fluid shear stresses rapidly with time constants in the range of 100 milliseconds[1]. However, RBCs lose their ability to deform dynamically with maladies such as diabetes[2,3], malaria infection[4–6], hereditary spherocytosis[7], and various mutations affecting globin genes, such as SCD[1,8]. Decrease in RBC deformability can drastically affect blood circulation due to increased viscosity[9]. Thus, probing RBC's dynamic deformability holds great potential for understanding the pathophysiology of various chronic, infectious, and genetic disorders, as well as for development of new monitoring and treatment regimens for these diseases.

SCD is the first recognized molecular disease, which was identified as a hemoglobin disorder more than 60 years ago[10]. In the roots of the disease is a point mutation in the sixth chain of the hemoglobin gene, which results in abnormal polymerization of hemoglobin molecules inside the RBCs[11]. Formation of polymerized hemoglobin fibers disrupts cell morphology, decreases RBC deformability (increase in stiffness) and changes membrane adhesive properties[11–14]. Abnormal adhesion and decreased deformability of RBCs are the main causes of blood vessel occlusion (vaso-occlusion) in SCD[11,13,15–18]. Vaso-occlusion is

[1]Case Biomanufacturing and Microfabrication Laboratory, Mechanical and Aerospace Engineering Department, Case Western Reserve University, Cleveland, OH 44106, USA, [2]Department of Hematology and Oncology, School of Medicine, Case Western Reserve University, Cleveland, OH 44106, USA, [3] Seidman Cancer Center at University Hospitals, Case Medical Center, Cleveland, OH, 44106, USA, [4]Biomedical Engineering Department, Case Western Reserve University, Cleveland, OH 44106, USA, [5]Department of Orthopaedics, Case Western Reserve University, Cleveland, OH 44106, USA, [6]Advanced Platform Technology Center, Louis Stokes Cleveland Veterans Affairs Medical Center, Cleveland, OH 44106, USA. *These authors contributed equally to this work. Correspondence should be addressed to U.A.G. (umut@case.edu).

Received 10 September 2015; accepted 8 December 2015; published online 19 February 2016; doi:10.1142/S2339547816400045

the hallmark of the disease and it has been associated with severe pain, crises, wide-spread organ damage, and early mortality[19,20].

Molecular basis of the SCD have been investigated extensively[21–24]. However, there are limited number of studies focusing on the biophysical factors in tandem, such as the deformability and the adhesion of RBCs, which are highly dynamic phenomena[8]. Even though RBC deformability has been associated with vaso-occlusion in SCD, we have limited knowledge on dynamic deformation characteristics of RBCs adhered to endothelium associated proteins in microphysiological fluid flow conditions.

Various approaches have been utilized to measure RBC deformability, including optical tweezers[25,26], micropipette aspiration[27], atomic force microscopy (AFM)[28,29], and microfluidics[8,18]. Even though optical tweezers, micropipette aspiration and AFM analyses have enabled sensitive and controlled measurement of RBC mechanical properties, these methods are typically performed in open environments without physiological fluid flow. On the other hand, microfluidic techniques allow incorporation of physiological flow conditions, as well as biologically relevant adhesion surfaces in a closed setting, which better mimic the natural physiological environment of the RBCs in blood flow. Previously, we have shown the heterogeneity of adhered sickle RBCs in terms of their deformability in quasi-static conditions, in a microfluidic environment[8].

Here, we present a microfluidic approach and a cell dimensioning algorithm to probe dynamic deformation behavior of adhered RBCs under physiological flow conditions at the single-cell level. Utilizing this approach, we probed the dynamic deformability of healthy hemoglobin A (HbA)- and homozygous HbS-containing RBCs using whole blood samples from 24 subjects. We defined a new parameter to evaluate dynamic deformability of RBCs: the dynamic deformability index (DDI), which is a function of the time dependent change of a cell's aspect ratio in response to fluid flow shear stress. We report for the first time on subpopulations of RBCs in terms of dynamic deformation characteristics in SCD: deformable and non-deformable adherent RBCs. Furthermore, we analyzed adhesion of non-deformable RBCs, in comparison to deformable RBCs, quantitatively at physiological and above physiological flow shear stresses in blood samples obtained from SCD patients. We observed significantly greater number of adhered non-deformable sickle RBCs than deformable sickle RBCs at flow shear stresses well above the physiological range, suggesting a potential interplay between dynamic deformability and increased adhesion of RBCs in vaso-occlusive events.

MATERIALS AND METHODS

Microfluidic device fabrication

The microfluidic system consisted of fibronectin (FN) functionalized glass surface, poly(methyl methacrylate) (PMMA, McMaster-Carr, Elmhurst, IL) top, and a 50-μm-thick double-sided adhesive (DSA) film (DSA, iTapestore, Scotch Plains, NJ) in the middle, defining the microchannel borders (**Fig. 1a**). The PMMA and DSA parts were micro-machined via VersaLaser system (Universal Laser Systems Inc., Scottsdale, AZ). The PMMA part encompassed inlets and outlets (0.61 mm in diameter and spaced 26 mm) of the microchannel. Channels were developed and operated to mimic the size scale and bulk flow conditions of post-capillary venules[8]. Wall shear stress for blood flow in post-capillary venules was estimated to be in the range of 1–5 dyne/cm^2.[14,30–32]

Surface chemistry of microfluidic channels

Microchannels were surface functionalized with FN to mimic the vascular wall surface. FN is an adhesive glycoprotein that is present on blood vessel wall surfaces. FN binds to RBC's integrin α4β1 receptor (also known as very late antigen-4 or VLA-4 integrin[33–35]) (**Fig. 1b**). FN proteins were immobilized in microfluidic channels through N-g-maleimidobutyryloxy succinimide ester (GMBS) coupling agent that is crosslinked to 3-aminopropyl triethoxysilane (APTES) molecules on the microchannel surface[8]. Briefly, GMBS stock and working solutions were prepared by dissolving 25 mg of GMBS in 0.25 mL DMSO, and diluting with ethanol to obtain 0.28% v/v ratio, respectively. FN working solution (100 μg/mL) was prepared by diluting the stock solution with phosphate buffer saline (PBS). Lyophilized bovine serum albumin (BSA) was dissolved in PBS (3 mg/mL), which was used to block the surface against non-specific adhesion. The microfluidic channels were rinsed with 30 μL of PBS and ethanol, and 20 μL of GMBS working solution was injected twice and incubated for 15 minutes at room temperature. Next, channels were rinsed twice with 30 μL of ethanol and PBS. Then, 20 μL of FN solution was injected into the microchannels and incubated for 1.5 hours at room temperature. The microfluidic channel surfaces were passivated by injecting 30 μL of BSA solution and incubated at 4°C overnight. Microchannels were rinsed with PBS immediately before blood sample processing.

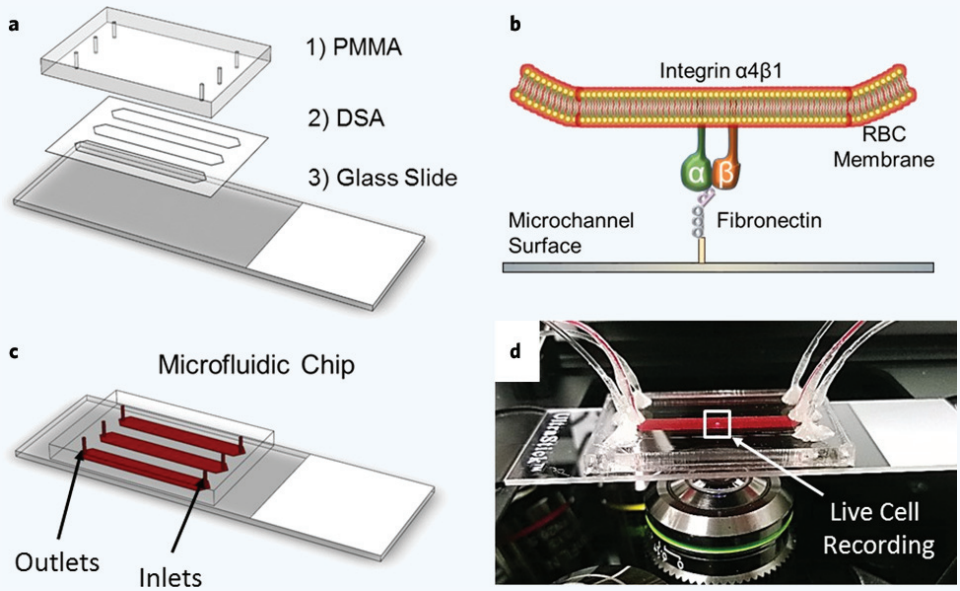

Figure 1 Microfluidic system for probing red blood cell (RBC) dynamic deformability. (**a**) Microfluidic system is composed of a poly(methyl methacrylate) (PMMA) cover, a double-sided adhesive (DSA) layer, which defines the channel shape and height (50 μm) and a glass slide base. (**b**) Microfluidic channels are functionalized with fibronectin, which mimics the microvasculature wall in a closed system and can process whole blood. (**c**) PMMA top cover in the microfluidic system comprises micromachined inlets and outlets for tubing connections and blood injection. (**d**) Microfluidic system is placed on an automated microscope stage for live cell image recording.

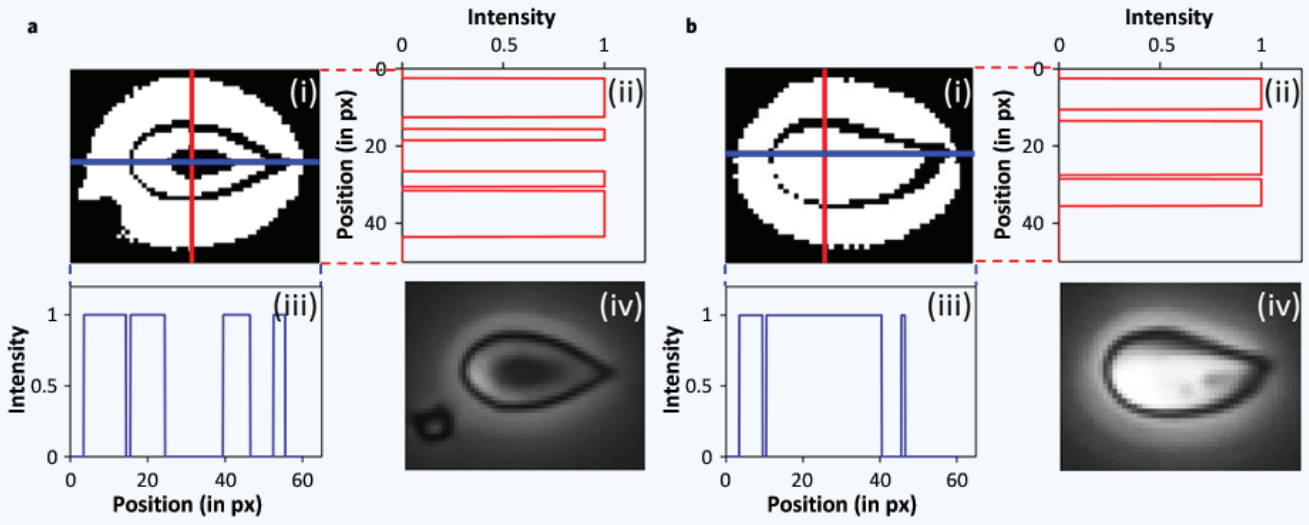

Figure 2 Automated dimensioning of adhered RBCs in microchannels. Length and width measurements of (**a**) deformable and (**b**) non-deformable RBCs. (**i**) Recorded single RBC images were converted to binary and the intensity threshold was adjusted to the level where the cell border was distinguishable. Vertical (**ii**) and horizontal (**iii**) intensity profiles along the binary image, where 0 represents black and 1 represents white. The length and width of the RBCs were determined using the outer edges of the black cell border. (**iv**) Unprocessed RBC images were cropped to contain the RBC of interest in the frame.

Blood processing in microchannels

Discarded de-identified patient blood samples were obtained from the Hematology and Oncology Division of University Hospitals under institutional review board (IRB) approval. Blood samples were collected in ethylenediaminetetraacetic acid (EDTA) anticoagulant vacutainer tubes and injected into microchannels, using disposable syringes, at precisely controlled flow shear stresses by using a syringe pump (New Era Inc., Farmingdale, NY). Whole blood samples without any dilution or pre-processing were used in the experiments. First, blood samples were introduced into the channels at 15.4 dyne/cm^2 until the microchannel was completely filled with blood (**Fig. 1c**); then, 15 µL of blood was pumped into the channel at a shear stress of 1.54 dyne/cm^2. After blood flow, channels were rinsed with flow cytometry buffer (R&D Systems, Minneapolis, MN) to remove non-adherent cells. For deformability analysis of single RBCs, an imaging area with adhered RBCs was selected and controlled shear stress with stepwise increments of 1 dyne/cm^2, up to 50 dyne/cm^2 was applied until the detachment of the RBCs was recorded. Microfluidic system design allowed us to precisely control fluid flow shear stress in a closed system, mimicking the physiological conditions of microvasculature. All the experiments were conducted at room temperature.

Microchannel visualization

The microfluidic device was placed on an Olympus IX83 inverted motorized microscope stage for live cell image recording and analysis during precisely controlled fluid flow (**Fig. 1d**). Olympus Cell Sense live-cell imaging and analysis software was utilized to obtain individual RBC recordings, as well as high-resolution images of the whole microfluidic channel with the adhered RBCs. Olympus (20×/0.45 ph2 and 40×/0.75 ph3) long working distance objective lenses were used for imaging, providing 445 µm × 332 µm and 223 µm × 166 µm imaging areas, respectively. Real-time videos of RBC deformations under applied fluid flow were recorded at 7 frames per second (fps) rate and converted to single-frame images for further processing and analysis.

Dynamic deformability analysis

Dimensions and cell aspect ratio (CAR) of single HbA (**Fig. 2a**) and HbS (**Fig. 2b**) RBCs were determined by image processing using a custom MATLAB code (Mathworks Inc., Natick, Massachusetts), which is provided in the supplementary information.

Briefly, each recorded frame was cropped to the size of the analyzed RBC (**Fig. 2a-iv,b-iv**). First, cropped frames were converted to binary and the centroids of the RBCs were determined (**Fig. 2a-i,b-i**). Then, intensity profiles along the vertical and horizontal axes were obtained and plotted through the centroid (**Fig. 2a-ii;iii,b-ii;iii**). Next, the data points from the plots were extracted and the points indicating the cell borders were used to determine the width and length of each RBC. Once all frames have been processed for each cell, RBC CARs were plotted against time, where time was calculated by the total number of frames divided by the fps rate. Developed image processing algorithm for determination of RBC dimensions and CAR provides accurate assessment of cell deformation in a time-efficient manner.

RESULTS AND DISCUSSION

We analyzed deformability of single HbA and HbS-containing RBCs by examining CAR for each individual frame that is recorded. Change in CAR, measured at no flow condition and at detachment instant (**Fig. 3a**), indicates deformability of RBCs. Healthy RBCs have a unique biconcave-discoid morphology, which plays a role in RBC's deformability and its passage through the microvasculature. We studied deformability of HbA and HbS-containing RBCs and observed subgroups of HbS containing RBCs: HbS deformable (with characteristic biconcave morphology) and HbS non-deformable (without characteristic biconcave morphology) (**Fig. 3a**).

CAR is a calculated ratio between the vertical width and the horizontal length of a cell (**Fig. 3b**). In response to fluid flow, HbA RBCs displayed an initial deformation (steep decrease in CAR), and then maintained their deformed state until cell detachment, which created a

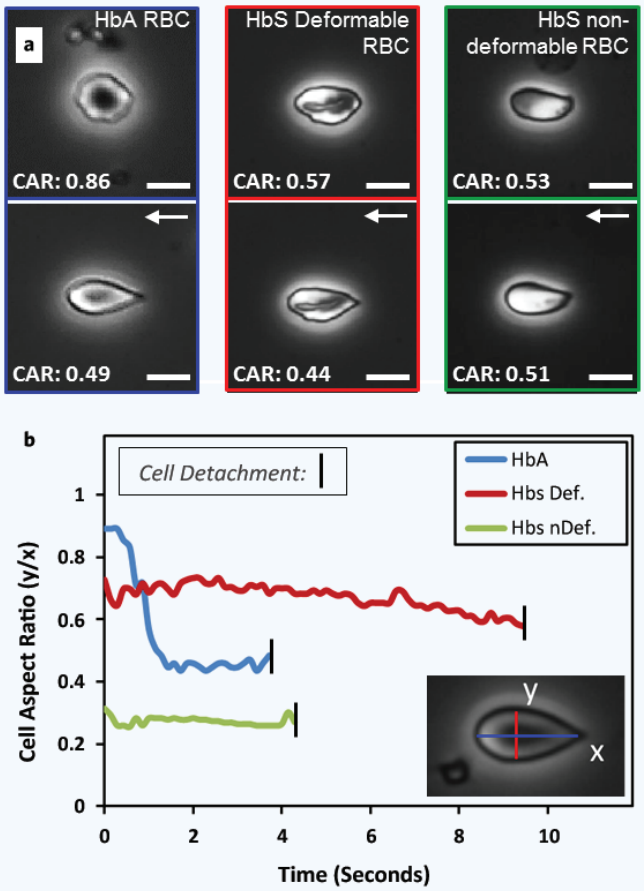

Figure 3 Dynamic deformability analysis of single RBCs containing healthy and sickle hemoglobin in microfluidic channels. (**a**) Different types of RBCs adhered on fibronectin functionalized surface in the absence of flow and right before detachment in response to applied flow. From left to right, healthy (HbA) RBCs, deformable HbS RBCs and non-deformable HbS RBCs, respectively. Scale bars represent 8 μm (length). Arrows indicate direction of flow. (**b**) Cell aspect ratio (CAR) change over time for typical HbA, deformable HbS and non-deformable HbS RBCs are shown. The CAR was calculated real-time by dividing the vertical width by the horizontal length (inset, y/x).

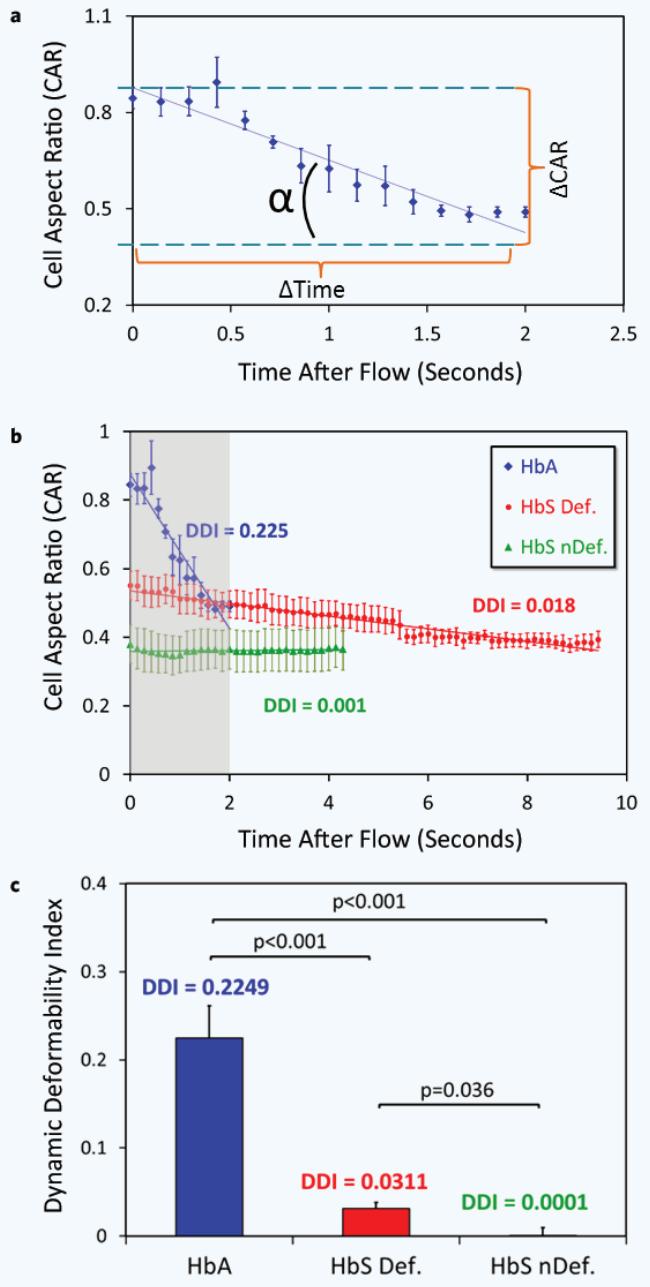

Figure 4 Dynamic deformability of healthy and sickle RBCs. (**a**) Dynamic deformability index (DDI) is determined as the rate of aspect ratio change in time in response to fluid shear stress. DDI = tan(α), where α is the angle between the change in CAR and the time of interest. (**b**) Healthy RBCs deformed at a much quicker rate and greater than non-deformable HbS and deformable HbS RBCs. Shown is the average curve for each group during deformation and the grey area indicates the time frame for when the HbA RBCs reached their deformed state. (**c**) The DDIs of each group were compared for the same amount of time (2 seconds, indicated by the grey area in b). The horizontal lines between individual groups represent statistically significant difference based on Kruskal–Wallis test followed by one-way ANOVA test with Fisher's post-hoc test for multiple comparisons (n = 3–6 cells in a total of 12 blood samples; $p < 0.05$). Error bars represent standard error of the mean.

plateau (**Fig. 3b**, typical deformation and detachment behavior is shown in **Supplementary Video 1** of the **Supplementary Information** section). On the other hand, deformable HbS RBCs displayed a continuous change in CAR until detachment, whereas non-deformable RBCs deformed negligibly (**Fig. 3b**).

We evaluated deformability of single RBCs in time from healthy and SCD subjects using DDI (**Fig. 4**). DDI was determined as the rate of aspect ratio change in time and calculated by Equation (1):

$$\mathrm{DDI} = \tan(\alpha), \qquad (1)$$

where α is the angle between the change in CAR and the time (**Fig. 4a**). For HbA RBCs, only the initial deformation region was taken into the account for DDI calculation, avoiding the plateau region (**Fig. 4b**). When RBCs were analyzed for deformation, healthy RBCs deformed at a much quicker rate and greater than deformable HbS RBCs (**Fig. 4b**). Both deformable HbA and HbS RBCs exhibited dynamic deformation until detachment, whereas non-deformable HbS RBCs demonstrated minimal dynamic deformation (**Fig. 4b**).

Next, DDI was determined for each cell type (**Fig. 4c**). HbA-containing RBCs showed significantly greater DDI than HbS-containing deformable and non-deformable RBCs after 2 seconds into deformation (**Fig. 4c**) (Kruskal–Wallis test followed by one-way ANOVA test, n = 3–6 cells in a total of 12 blood samples; $p < 0.05$). Deformable HbS-containing

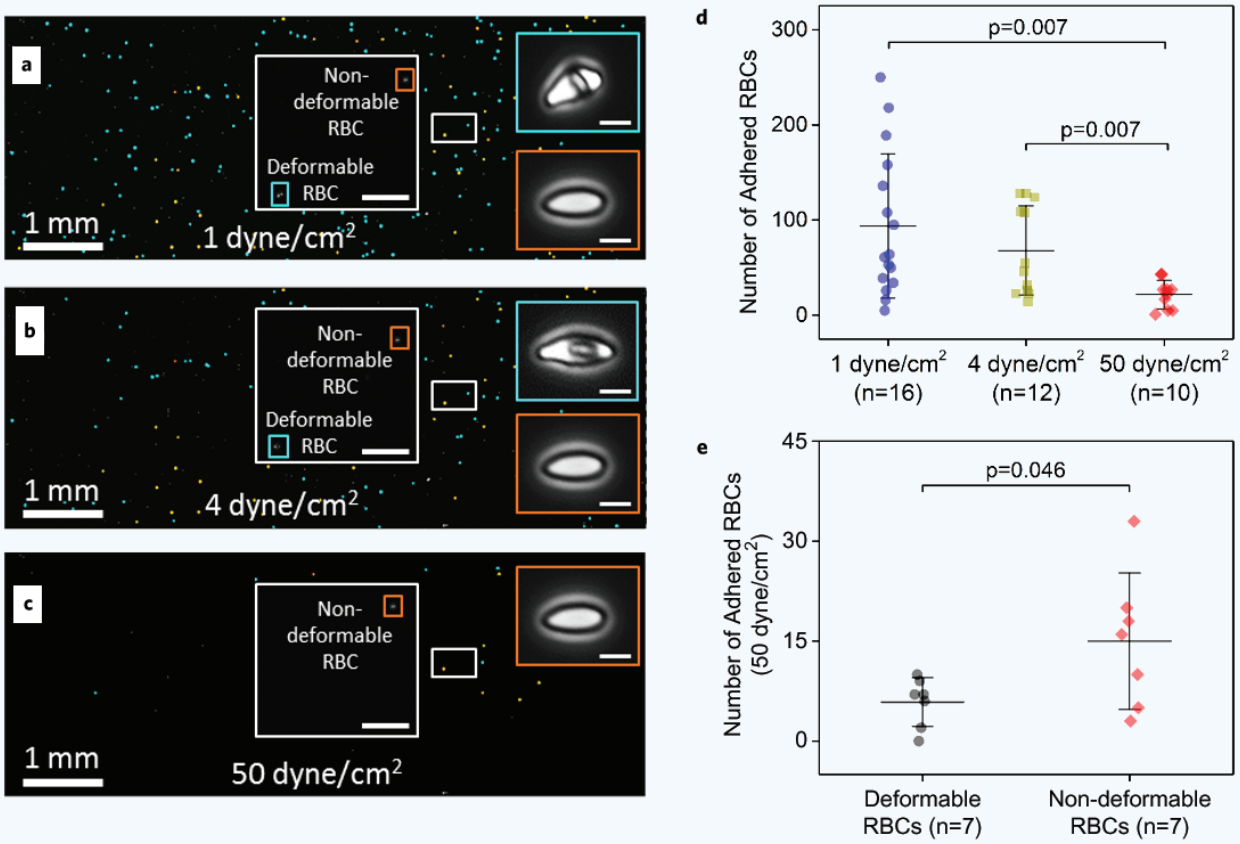

Figure 5 Subpopulations of sickle RBCs based on adhesion and deformability in microphysiological flow. (**a**–**c**) Number of adhered RBCs and morphologies were analyzed at step-wise increased shear stresses of (**a**) 1 dyne/cm^2, (**b**) 4 dyne/cm^2 and (**c**) 50 dyne/cm^2. Deformable (with characteristic biconcave shape) and non-deformable RBCs (without characteristic biconcave shape) were determined based on morphological characterization. Scale bars represent 50 µm and 5 µm (length) in insets, respectively. (**d**) Number of adhered RBCs were significantly lower at 50 dyne/cm^2 shear stress compared to shear stresses of 1 dyne/cm^2 and 4 dyne/cm^2. (**e**) Number of adhered non-deformable RBCs at 50 dyne/cm^2 shear stress was significantly higher than number of adhered deformable RBCs. The horizontal lines between individual groups represent statistically significant difference based on a one-way ANOVA test with Fisher's post-hoc test for multiple comparisons ($p < 0.05$). *n* represents the number of subjects. Data point crossbars represent the mean and error bars represent the standard error of the mean.

RBCs displayed significantly higher DDI than non-deformable HbS-containing RBCs (**Fig. 4c**) ($p < 0.05$). These results showed a significant difference in dynamic deformability between healthy and sickle RBCs. Furthermore, our findings suggest that there exist subpopulations of HbS-containing RBCs based on DDI.

Next, we analyzed the adhesion of HbS-containing RBCs in SCD patient blood samples to FN immobilized microfluidic channels under controlled physiological flow shear stresses (**Fig. 5**). The number of adhered RBCs was quantified at shear stresses of 1 dyne/cm^2, 4 dyne/cm^2, and 50 dyne/cm^2 (**Fig. 5a–c**). Adhered RBCs were categorized as either: (i) deformable with characteristic biconcave morphology or (ii) non-deformable without characteristic biconcave morphology (**Fig. 5a–c**). We observed a decrease in the number of adhered RBCs with increased flow shear stresses (**Fig. 5d**). The number of adhered RBCs was significantly lower at 50 dyne/cm^2 shear stress, in comparison with shear stresses of 1 dyne/cm^2 and 4 dyne/cm^2 (**Fig. 5d**, one-way ANOVA test with Fisher's post-hoc test for multiple comparisons; $p < 0.05$). These findings indicate subpopulations of RBCs in terms of adhesion strength to FN functionalized surface.

Despite the decreased number of adhered RBCs at 50 dyne/cm^2, we observed a subset of RBCs remaining adhered to the microchannel surface. Then, we quantified the number of adhered deformable and non-deformable RBCs in this subset. We observed a significantly greater number of non-deformable HbS RBCs compared to deformable RBCs that adhered at a flow shear stress level (i.e. 50 dyne/cm^2) well above the physiological range (one-way ANOVA test with Fisher's post-hoc test for multiple comparisons; $p < 0.05$). These results suggest an interplay between dynamic deformability and increased adhesion of RBCs.

In mammals, the RBC has uniquely evolved to lose its nucleus and organelles to become remarkably flexible[36]. RBC's adherence to vascular wall and other cells is insignificant[1], while most other cell types depend on adhesive interactions to survive[37]. A typical RBC travels about 300 miles in its lifespan of about 120 days in the body without jamming the microcirculation[1]. An RBC repeatedly deforms and squeezes through narrow capillaries that can be as small as half of its diameter[1,38,39]. The associations between RBC's adhesion and its deformability are not fully understood.

SCD is a genetically inherited disease that is associated with considerable cost, morbidity, and mortality[20,40]. Molecular events taking place in the disease pathophysiology is very well recognized. However, the links between these molecular changes and the response in mesoscale cell biophysical properties and the macroscale vasculature events affecting blood

circulation are yet to be discovered[41,42]. On the other hand, biophysical alterations happening at the cellular level can potentially reflect the progression of the disease. In this study, we showed significantly greater adhesion, both qualitatively and quantitatively, of RBCs with diminished deformation capabilities. These results may indicate a critical role for non-deformable RBCs in vaso-occlusion due to their strong adhesion at flow shear stresses well above the physiological range.

The contribution of different cell types in initiation and propagation of the vaso-occlusion are still under investigation. Earlier literature has suggested that vaso-occlusion is initiated by the adhesion of reversibly sickled deformable RBCs, and propagated with the trapping and adhesion of irreversibly sickled non-deformable RBCs, resulting in reduced blood flow and obstruction[14,43]. In our study, we observed significantly greater number of adhered non-deformable RBCs compared to deformable RBCs at a shear stress (50 dyne/cm^2) well above the physiological range (1–5 dyne/cm^2). The fact that non-deformable sickle RBCs remained adhered at high shear stresses indicates their enhanced adhesion characteristics, which can be indicative of their critical role in vaso-occlusion. Furthermore, stronger adhesion of RBCs with decreased deformability supports the idea that cyclic polymerization of HbS induces rearrangement of membrane proteins and membrane protrusions, resulting in increased adhesion[11,44,45].

It is still not clear which proteins are the most critical in mediating cellular adhesive events in vaso-occlusion. This is partly due to the complex nature of interactions between blood cells and the endothelium[33,46]. Most studies on sickle RBC adhesion have been conducted with extensive sample preparation protocols, such as washing and excessive dilutions, potentially compromising the effect of autologous plasma on adhesive events. Lack of plasma proteins in these studies, could have masked various interactions. FN has been shown to mediate sickle RBC adhesion with endothelial damage and inflammatory activation[34,46]. In blood vessels, FN can be found in three forms: (i) as sub-endothelial matrix protein, (ii) as soluble in plasma or (iii) as bound on endothelial cells[34,47]. Furthermore, multiple reports suggest that fibronectin plays a role in sickle RBC adhesion[33,46,48–50]. In this study, we selected FN based on earlier studies and due to its potential clinical relevance in SCD.

A limitation of this study is the use of discarded de-identified patient blood samples, due to which patient's clinical status was not associated with the findings. Patient's clinical status would include the disease severity and treatment modality, including transfusion or hydroxyurea. For example, hydroxyurea is the only U.S. Food and Drug Administration (FDA)-approved drug for the management of SCD, which increases hemoglobin F (HbF) content in RBCs. Increased intracellular HbF molecules interferes with sickle hemoglobin polymerization and prevents any subsequent deleterious effects on RBC membrane. Since hydroxyurea treatment has been shown to decrease RBC adhesion in the literature[51,52], it is plausible that blood samples of patients under hydroxyurea treatment will possess less adherent RBCs. We will investigate these aspects in future clinical studies with consented SCD patients.

Molecular events alter cellular composition and properties, and these changes in RBCs collectively affect circulation, which will retrospectively have an impact on RBCs. In SCD, initial obstruction of blood flow in venules due to increased adhesion and reduced deformability of sickle RBCs leads to further hypoxia, which in return causes further sickling and further hypoxia. This phenomenon is also known as the vicious cycle[11,53]. Thus, accurate measurement of RBC deformability and adhesion, which are the two key factors in vaso-occlusion, hold great potential as a marker for assessment of disease progression, for gaining insight into disease pathophysiology, and for development of novel therapeutics.

CONCLUSIONS

In summary, we present a microfluidic system integrated with an image processing algorithm to probe DDI of adhered RBCs. Based on DDI, we report subpopulations of HbS-containing RBCs. A unified investigation of adhesion and deformability properties of RBCs may have significant implications for understanding vaso-occlusion events and for phenotyping disease pathophysiology. The microfluidic system described here has the potential to be used in a high-throughput manner with an integrated automated image processing algorithm that determines DDI of individual adhered RBCs. Studying dynamic deformation of cells may have implications in other multi-system diseases such as β-thalassemia, diabetes mellitus, hereditary spherocytosis, polycythemia vera, and malaria.

ACKNOWLEDGEMENTS

This work was supported by Grant No. 2013126 from the Doris Duke Charitable Foundation. The authors acknowledge with gratitude the contributions of patients and clinicians at the Seidman Cancer Center (University Hospitals, Cleveland). The authors also acknowledge Grace Gongaware, a student at the Cleveland Institute of Art for crafting the scientific illustrations. U.A.G. would like to thank the Case Western Reserve University, University Center for Innovation in Teaching and Education (UCITE) for the Glennan Fellowship, which supports the scientific art program and the art student internship at Case Biomanufacturing and Microfabrication Laboratory.

AUTHORSHIP CONTRIBUTIONS

Y.A. and U.A.G. developed the idea; Y.A., Y.M. and U.A.G. designed the experiments; Y.A. and Y.M. performed the experiments; Y.A., Y.M. and U.A.G. analyzed the results; Y.A., Y.M. and U.A.G. prepared the figures and the supplementary information; and Y.A., Y.M., J.A.L. and U.A.G. wrote the manuscript.

DISCLOSURE OF CONFLICTS OF INTEREST

The authors declare no competing financial interests. Y.A., J.A.L. and U.A.G. filed a patent application pertaining to the results presented in this paper: Patent Cooperation Treaty Application (PCT/US2015/042907): "Biochips to Diagnose Hemoglobin Disorders and Monitor Blood Cells".

REFERENCES

1. Mohandas, N. & Gallagher, P.G. Red cell membrane: Past, present, and future. *Blood* **112**, 3939–3948 (2008).
2. Juhan, I. *et al.* Abnormalities of erythrocyte deformability and platelet aggregation in insulin-dependent diabetics corrected by insulin *in vivo* and *in vitro*. *Lancet* **1**, 535–537 (1982).
3. Diamantopoulos, E.J. *et al.* Impaired erythrocyte deformability precedes vascular changes in experimental diabetes mellitus. *Horm. Metab. Res.* **36**, 142–147 (2004).
4. Huang, S. *et al.* Dynamic deformability of *Plasmodium falciparum*-infected erythrocytes exposed to artesunate *in vitro*. *Integr. Biol.* **5**, 414–422 (2013).
5. Glenister, F.K., Coppel, R.L., Cowman, A.F., Mohandas, N. & Cooke, B.M. Contribution of parasite proteins to altered mechanical properties of malaria-infected red blood cells. *Blood* **99**, 1060–1063 (2002).
6. Cooke, B.M., Mohandas, N. & Coppel, R.L. Malaria and the red blood cell membrane. *Semin. Hematol.* **41**, 173–188 (2004).
7. Perrotta, S., Gallagher, P.G. & Mohandas, N. Hereditary spherocytosis. *Lancet* **372**, 1411–1426 (2008).
8. Alapan, Y., Little, J.A. & Gurkan, U.A. Heterogeneous red blood cell adhesion and deformability in sickle cell disease. *Sci. Rep.* **4**, 7173 (2014).
9. Kim, Y., Kim, K. & Park, Y. *Measurement Techniques for Red Blood Cell Deformability: Recent Advances* (InTech, 2012).
10. Pauling, L., Itano, H.A. *et al.* Sickle cell anemia a molecular disease. *Science* **110**, 543–548 (1949).
11. Barabino, G.A., Platt, M.O. & Kaul, D.K. Sickle cell biomechanics. *Ann. Rev. Biomed. Eng.* **12**, 345–367 (2010).
12. Kaul, D.K., Fabry, M.E. & Nagel, R.L. Microvascular sites and characteristics of sickle cell adhesion to vascular endothelium in shear flow conditions: Pathophysiological implications. *Proc. Natl. Acad. Sci. U. S. A.* **86**, 3356–3360 (1989).
13. Hebbel, R.P., Boogaerts, M.A., Eaton, J.W. & Steinberg, M.H. Erythrocyte adherence to endothelium in sickle-cell anemia. A possible determinant of disease severity. *N. Engl. J. Med.* **302**, 992–995 (1980).
14. Kaul, D.K., Finnegan, E. & Barabino, G.A. Sickle red cell-endothelium interactions. *Microcirculation* **16**, 97–111 (2009).

15. Evans, E., Mohandas, N. & Leung, A. Static and dynamic rigidities of normal and sickle erythrocytes. Major influence of cell hemoglobin concentration. *J. Clin. Invest.* **73**, 477–488 (1984).
16. Nash, G.B., Johnson, C.S. & Meiselman, H.J. Mechanical properties of oxygenated red blood cells in sickle cell (HbSS) disease. *Blood* **63**, 73–82 (1984).
17. Brandao, M.M. *et al.* Optical tweezers for measuring red blood cell elasticity: Application to the study of drug response in sickle cell disease. *Eur. J. Haematol.* **70**, 207–211 (2003).
18. Zheng, Y. *et al.* Mechanical differences of sickle cell trait (SCT) and normal red blood cells. *Lab Chip* **15**, 3138–3146 (2015).
19. Hofrichter, J., Ross, P.D. & Eaton, W.A. Kinetics and mechanism of deoxyhemoglobin S gelation: A new approach to understanding sickle cell disease. *Proc. Natl. Acad. Sci. U. S. A.* **71**, 4864–4868 (1974).
20. Platt, O.S. *et al.* Mortality in sickle cell disease. Life expectancy and risk factors for early death. *N. Engl. J. Med.* **330**, 1639–1644 (1994).
21. Stuart, M.J. & Nagel, R.L. Sickle-cell disease. *Lancet* **364**, 1343–1360 (2004).
22. Noguchi, C.T. & Schechter, A.N. Sickle hemoglobin polymerization in solution and in cells. *Annu. Rev. Biophys. Biophys. Chem.* **14**, 239–263 (1985).
23. Ferrone, F.A. Polymerization and sickle cell disease: A molecular view. *Microcirculation* **11**, 115–128 (2004).
24. Dean, J. & Schechter, A.N. Sickle-cell anemia: Molecular and cellular bases of therapeutic approaches (first of three parts). *N. Engl. J. Med.* **299**, 752–763 (1978).
25. Rancourt-Grenier, S. *et al.* Dynamic deformation of red blood cell in dual-trap optical tweezers. *Opt. Express* **18**, 10462–10472 (2010).
26. Dao, M., Lim, C.T. & Suresh, S. Mechanics of the human red blood cell deformed by optical tweezers. *J. Mech. Phys. Solids* **51**, 2259–2280 (2003).
27. Sinha, A., Chu, T.T., Dao, M. & Chandramohanadas, R. Single-cell evaluation of red blood cell bio-mechanical and nano-structural alterations upon chemically induced oxidative stress. *Sci. Rep.* **5**, 9768 (2015).
28. Chen, X., Feng, L., Jin, H., Feng, S. & Yu, Y. Quantification of the erythrocyte deformability using atomic force microscopy: Correlation study of the erythrocyte deformability with atomic force microscopy and hemorheology. *Clin. Hemorheol. Microcirc.* **43**, 243–251 (2009).
29. Bremmell, K.E., Evans, A. & Prestidge, C.A. Deformation and nano-rheology of red blood cells: An AFM investigation. *Colloid Surface B* **50**, 43–48 (2006).
30. Sheikh, S., Rainger, G.E., Gale, Z., Rahman, M. & Nash, G.B. Exposure to fluid shear stress modulates the ability of endothelial cells to recruit neutrophils in response to tumor necrosis factor-alpha: A basis for local variations in vascular sensitivity to inflammation. *Blood* **102**, 2828–2834 (2003).
31. Shaik, S.S. *et al.* Low intensity shear stress increases endothelial ELR+ CXC chemokine production via a focal adhesion kinase-p38{beta} MAPK-NF-{kappa}B pathway. *J. Biol. Chem.* **284**, 5945–5955 (2009).
32. Kang, H., Kwak, H.I., Kaunas, R. & Bayless, K.J. Fluid shear stress and sphingosine 1-phosphate activate calpain to promote membrane type 1 matrix metalloproteinase (MT1-MMP) membrane translocation and endothelial invasion into three-dimensional collagen matrices. *J. Biol. Chem.* **286**, 42017–42026 (2011).
33. Kasschau, M.R., Barabino, G.A., Bridges, K.R. & Golan, D.E. Adhesion of sickle neutrophils and erythrocytes to fibronectin. *Blood* **87**, 771–780 (1996).
34. Kumar, A., Eckmam, J.R., Swerlick, R.A. & Wick, T.M. Phorbol ester stimulation increases sickle erythrocyte adherence to endothelium: A novel pathway involving alpha 4 beta 1 integrin receptors on sickle reticulocytes and fibronectin. *Blood* **88**, 4348–4358 (1996).
35. Wick, T.M. & Eckman, J.R. Molecular basis of sickle cell–endothelial cell interactions. *Curr. Opin Hematol.* **3**, 118–124 (1996).
36. Sprague, R.S., Stephenson, A.H. & Ellsworth, M.L. Red not dead: Signaling in and from erythrocytes. *Trends Endocrinol. Metab.* **18**, 350–355 (2007).
37. Meredith, J.E., Fazeli, B. & Schwartz, M.A. The extracellular–matrix as a cell-survival factor. *Mol. Biol. Cell* **4**, 953–961 (1993).
38. Skalak, R. & Branemar P.I. Deformation of red blood cells in capillaries. *Science* **164**, 717–719 (1969).
39. Canham, P.B. & Burton, A.C. Distribution of size and shape in populations of normal human red cells. *Circ. Res.* **22**, 405–422 (1968).
40. Ballas, S.K. The cost of health care for patients with sickle cell disease. *Am. J. Hematol.* **84**, 320–322 (2009).
41. Wood, D.K., Soriano, A., Mahadevan, L., Higgins, J.M. & Bhatia, S.N. A biophysical indicator of vaso-occlusive risk in sickle cell disease. *Sci. Transl. Med.* **4**, 123–126 (2012).
42. Aprelev, A. *et al.* Sickle cell occlusion in microchannels. In Herold, K., Vossoughi, J. & Bentley, W. eds. *26th Southern Biomedical Engineering Conference SBEC 2010*, Vol. 32, Ch. 137, pp. 536–539 (Springer, 2010).
43. Manwani, D. & Frenette, P.S. Vaso-occlusion in sickle cell disease: Pathophysiology and novel targeted therapies. *Blood* **122**, 3892–3898 (2013).
44. Frenette, P.S. & Atweh, G.F. Sickle cell disease: Old discoveries, new concepts, and future promise. *J. Clin. Invest.* **117**, 850–858 (2007).
45. Kaul, D.K. Vascular obstruction in sickle cell disease. *Einstein J. Biol. Med.* **18**, 156–163 (2001).
46. Manodori, A.B. Sickle erythrocytes adhere to fibronectin-thrombospondin-integrin complexes exposed by thrombin-induced endothelial cell contraction. *Microvasc. Res.* **61**, 263–274 (2001).
47. Cartron, J.P. & Elion, J. Erythroid adhesion molecules in sickle cell disease: Effect of hydroxyurea. *Transfus. Clin. Biol.* **15**, 39–50 (2008).
48. Lutty, G.A. *et al.* Mechanisms for sickle red blood cell retention in choroid. *Curr. Eye Res.* **25**, 163–171 (2002).
49. Lutty, G.A. *et al.* Inhibition of TNF-alpha-induced sickle RBC retention in retina by a VLA-4 antagonist. *Invest. Ophthalmol. Vis. Sci.* **42**, 1349–1355 (2001).
50. Montes, R.A., Eckman, J.R., Hsu, L.L. & Wick, T.M. Sickle erythrocyte adherence to endothelium at low shear: Role of shear stress in propagation of vaso-occlusion. *Am. J. Hematol.* **70**, 216–227 (2002).
51. Rosse, W.F., Narla, M., Petz, L.D. & Steinberg, M.H. New Views of sickle cell disease pathophysiology and treatment. *Hematology: The Education Program of the American Society of Hematology. American Society of Hematology* pp. 2–17 (2000).
52. Halsey, C. & Roberts, I.A. The role of hydroxyurea in sickle cell disease. *Br. J. Haematol.* **120**, 177–186 (2003).
53. Verduzco, L.A. & Nathan, D.G. Sickle cell disease and stroke. *Blood* **114**, 5117–5125 (2009).

SUPPLEMENTARY INFORMATION

Image processing algorithm was developed in Matlab as shown below:

```
Clear

%This program will read through the entire folder.
imagefiles = dir('*.tif');

%read images
w = [];
h = [];
files = 27;%number of files in folder, basically number of frames
for number = 1:files
filename =imagefiles(number).name;
    I=imread(filename);

%crop image so just the cell of interest remains in the frame. Since the
%image sizes are big, Matlab will take longer if you work with them at full
%size. Also regionprops function would not be able to detect the specific object as
%well.
CroppedI = imcrop(I,[695.5 530.5 82 63]);
subplot(2,2,1)
imshow(CroppedI)
title('Original Image')
```

```
%make the image binary - this will help when looking for intensity
%later on, as well as finding centroids.
%level = graythresh(CroppedI);
% ^ another way to find level instead of manually changing it
bw = im2bw(CroppedI,0.21);
bw = bwareaopen(bw, 50);
subplot(2,2,2)
imshow(bw)
title('Binary Image')

%Find the centroid of the cell and mark it
measurements = regionprops(bw, 'Centroid');
mc = [];
mc = measurements.Centroid;
hold on;
  plot(mc(1), mc(2), 'r+', 'MarkerSize', 120, 'LineWidth', 1);

  hold off;

x = mc(1);
y = mc(2);

%improfile finds the intensity along a set path. The higher the number,
%the closer it is to white, and lower the number, the closer it is to black.
%Since the image was converted to binary, the possible numbers are 1 and 0,
%which makes the process a lot smoother to determine the borders of the cells.
%All the RBCs have a black background, white glowing border around them, a
%thin line of black for the actual cell border, another white region between
%cell wall. When the horizontal and vertical lines are drawn across the
%centroids for the intensities, it will start off as 0 (black bg), then 1
%(white glow), then a spike to 0 (cell wall),then back up 1, and the second
%to last spike to 0 is the other side of the cell wall.

%Getting the width of the cell
subplot(2,2,3)
improfile(bw, [0 90], [y y], 1000); %finds horizontal intensity
title('Horizontal Intensity');
%data points of plot for length
YDataw=get(get(gca,'children'),'YData');
XDataw=get(get(gca,'children'),'XData');

firstw = [];
lastw = [];

%find the 0 spikes
for i = 2:length(XDataw)
    %the first border - first 0 when the point before is 1
    if YDataw(i)==0 && YDataw(i-1)==1
       firstw = [firstw, XDataw(i)];
    end
    %the second border - last 0 when the point after is 1
    if YDataw(i)==0 && YDataw(i+1) == 1
        lastw = [lastw, XDataw(i)];
    end
end
width = lastw(length(lastw)) - firstw(1);
w = [w, width];

%Getting the height of the cell
subplot(2,2,4)
improfile(bw, [x x], [0 90], 1000);%finds vertical intensity
%data points of plot with width
title('Vertical Intensity');
YDatah=get(get(gca,'children'),'YData');
```

```
XDatah=get(get(gca,'children'),'XData');

firsth = [];
lasth = [];


%find the 0 spikes
for i = 2:length(XDatah)
    %the first border - first 0 when the point before is 1
    if YDatah(i)==0 && YDatah(i-1)==1
       firsth = [firsth, XDatah(i)];
    end
    %the second border - last 0 when the point after is 1
    if YDatah(i)==0 && YDatah(i+1) == 1
        lasth = [lasth, XDatah(i)];
    end
end

height = lasth(length(lasth)) - firsth(1);
h = [h, height];
end

%Convert from pixels to micrometer.

h2 = h*8/h(1);
w2 = w*8.97/w(1);

time = linspace(0,files/7,files); %Divide by 7 since video was 7fps
figure, plot(time,h2,time,w2)
xlabel(' Time After Flow to Release (Seconds)');
ylabel('Length of Width/Height (Micrometer)');
legend('Height Change', 'Width Change');

%plot aspect ratio
ar = [];
for a = 1:length(h2)
    ratio = h2(a)/w2(a);
    ar = [ar, ratio];
end
figure, plot(time,ar)
ylabel('Cell Aspect Ratio');
xlabel('After Flow to Release (Seconds)');
title('Change in Cell Aspect Ratio with Respect to Time');

%deformability index
di = [];
for d = 1:length(h2)
    deform = (h2(d)-w2(d))/(h2(d)+w2(d));
    di = [di, deform];
end
figure, plot(time, di);
xlabel('After Flow to Release (Seconds)');
title('Deformability Index');
```

Supplementary Video 1 Deformation and detachment of a typical adhered RBC. Scale bar represents 3.6 μm (length). [Multimedia View] Can be viewed at http://www.worldscientific.com/doi/suppl/10.1142/S2339547816400045